Excitation of a nonlinear plasma ion wake by intense energy sources with applications to the crunch-in regime

Aakash A. Sahai*

Department of Physics, Blackett Laboratory and John Adams Institute for Accelerator Sciences, Imperial College London, London, SW7 2AZ, United Kingdom, and Department of Electrical Engineering, Duke University, Durham, North Carolina 27708, USA

(Received 5 February 2017; published 23 August 2017)

We show the excitation of a nonlinear ion-wake mode by plasma electron modes in the bubble regime driven by intense energy sources, using analytical theory and simulations. The ion wake is shown to be a driven nonlinear ion-acoustic wave in the form of a long-lived cylindrical ion soliton which limits the repetition rate of a plasma-based particle accelerator in the bubble regime. We present the application of this evacuated and radially outwards propagating ion-wake channel with an electron skin-depth scale radius for the "crunch-in" regime of hollow-channel plasma. It is shown that the time-asymmetric focusing force phases in the bubble couple to ion motion significantly differently than in the linear electron mode. The electron compression in the back of the bubble sucks in the ions whereas the space charge within the bubble cavity expels them, driving a cylindrical ion-soliton structure at the bubble radius. Once formed, the soliton is sustained and driven radially outwards by the thermal pressure of the wake energy in electrons. Particle-in-cell simulations are used to study the ion-wake soliton structure, its driven propagation and its use for positron acceleration in the crunch-in regime.

DOI: 10.1103/PhysRevAccelBeams.20.081004

I. INTRODUCTION

Plasma ions are generally assumed to be stationary in the theory of ultrarelativistic plasma electron waves [1]. Such waves are regularly excited by high-intensity energy sources such as an ultrashort laser or particle beams [2] and have proven to be promising for accelerating and transporting beams with 10^9 Vm^{-1} field strengths. The nonlinear regime of cavitated electron "bubble" modes [3–5] of these waves which rely on the immobility of ions for exciting charge-separation fields, have been proposed to form the basis of plasma colliders [6].

Important exceptions to the fundamental assumption of stationary ions occur as the intensities of the energy sources become high enough (for instance in the final stage of envisioned plasma-based collider designs) to lead to significant ion trajectories within a period of the electron wave [7]. Ion motion also invariably becomes important over several periods of the electron wake train further behind the driver because as we will show the energy left over in the electron oscillation modes couples to the ion modes. This long-term evolution of wakefields in plasma [8] constrains the repetition rate of colliders or light sources that use plasma-based acceleration, and is the primary motivation for this work.

This work is fundamental and important from two different perspectives: (i) it is the first analytical consideration of an ion-wake driven by the bubble regime of electron plasma waves. Our work proves the excitation and persistence of a radially propagating cylindrical ion soliton-like mode. It is shown to be directly excited by the bubble fields, unlike the ion motion driven behind a linear electron wake. Its radial motion is sustained by the thermalizing wake energy in electrons. (ii) We show that an ion-wake channel, which can be meter scale for the beam-driven plasma electron waves, can be used for a novel hollow-channel mode in the "crunch-in" regime [9,10]. The evacuation of electrons and ions behind the soliton results in a channel-like ion-wake structure which persists over many hundreds of plasma electron periods and is here shown to be suitable for exciting nonlinear hollow-channel electron modes driven by relativistic positron and electron beams, first investigated by the author.

Ion wake is analyzed theoretically and using computational modeling, to show that it is the time asymmetry of the phases of the focusing fields of the bubble which leads to the excitation of a nonlinear ion-acoustic mode in the form of a cylindrical ion soliton. Its characteristics are similar to the solutions of the cylindrical Korteweg–de Vries equation (cKdV) [11–14]. The bubble electron mode may be driven by any type of an ultrashort high energy-density energy source such as an intense laser [15] or a particle beam [16]. This work gains a distinct importance because the bubble

*aakash.sahai@gmail.com

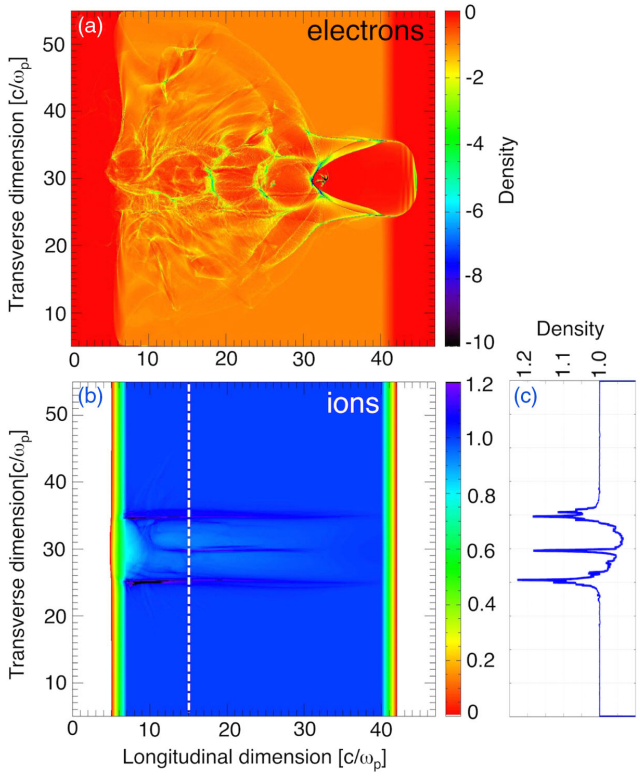

FIG. 1. Laser driven nonlinear ion wake at early time ($t = 46\omega_{\rm pe}^{-1} = 0.17 f_{\rm pi}^{-1}$, where $f_{\rm pi}$ is the plasma ion frequency) in $m_i = m_p = 1836 m_e$ plasma. (a) Electron bubble mode in Cartesian coordinates (fixed box) with $\frac{\omega_0}{\omega_{\rm pe}} = 10$ driven by a matched laser pulse (vector potential $a_0 = 4$ and frequency ω_0) with $R_B \simeq 4\frac{c}{\omega_{\rm pe}}$. (b) Nonlinear ion wake in the form of a cylindrical ion-soliton of radius $\simeq 4\frac{c}{\omega_{\rm pe}}$ excited behind the bubble electron wake in a proton plasma. (c) Transverse ion-density profile at $z = 15c/\omega_{\rm pe}$. Notice that the ion density perturbation in this excitation phase is still building up and is a fraction of the background ion density, $\frac{\delta n_i}{n_0} < 1$.

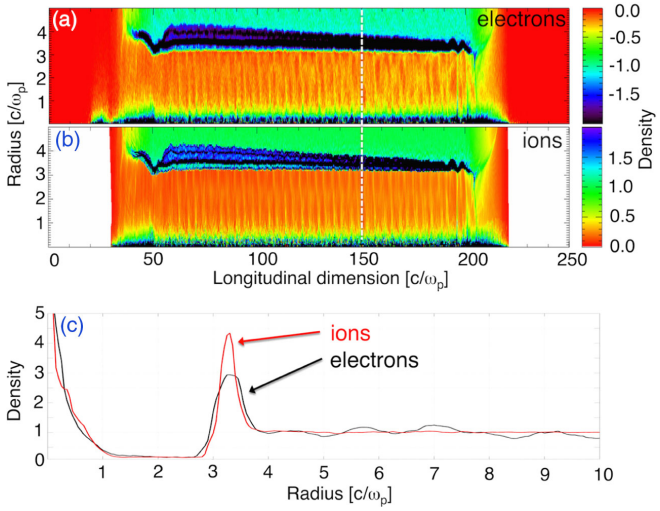

FIG. 2. Electron beam-driven nonlinear ion wake at late time ($t = 460\omega_{\rm pe}^{-1} = 1.7 f_{\rm pi}^{-1}$) in $m_i = m_p = 1836 m_e$ plasma. (a) Beam-driven ion-wake electron density in cylindrical coordinates (fixed box). The beam parameters are $n_b = 5n_0$, $\sigma_r = 0.5c/\omega_{\rm pe}$, $\sigma_z = 1.5c/\omega_{\rm pe}$, $\gamma_b = 38,000$, these beam-plasma parameters are quite similar to [5]. (b) Corresponding ion density in cylindrical coordinates (fixed box). Note the N-soliton formation in the ion density, $50c/\omega_{\rm pe} \le z \le 100c/\omega_{\rm pe}$. The later times in the time evolution of the ion wake are also inferred from density snapshots farther behind the beam. (c) Radial electron and ion density profile at $z = 150c/\omega_{\rm pe}$. A full movie of radial electron and ion density dynamics is presented in Supplemental Material [20].

regime is the underlying acceleration mode for future plasma-based colliders, but there is currently no understanding of the long-term behavior of the plasma [8,17] which determines its state for the succeeding bunches, defining an upper limit on the repetition rate.

The critical result of this work is the fact that the ion wake is a cylindrical solitonlike mode which is self-reinforcing collective motion of ions, resulting in considerable lengthening of its lifetime in comparison to an entirely randomized ion motion. The long-lived ion-mode leftover in the plasma is tracked over many hundreds of electron periods in simulations. This establishes its persistence for hundreds of picosecond time scale for an operating plasma density of 10^{17} cm^{-3}.

The excitation of crunch-in using the nonlinear ion-wake mode for plasma-based acceleration in a hollow channel using positron beam is demonstrated. The crunch-in regime in an ideal hollow channel using positron beams was first introduced in [9,10] and Chapter 8 of [18]. In this regime, the excitation of strong focusing fields was shown in complete contrast to the conventionally established conclusion that relativistic particles excite zero focusing fields in a hollow channel [19]. The ion-wake channel-wall electrons collapse towards the energy-propagation axis resulting in a nonlinear on-axis electron density compression. The optimal compression is shown to be only possible if the driving beam properties are matched to the channel radius [9], a strong characteristic dependence on the excitation which is a signature of nonlinearity. The choice of an appropriate channel radius is enabled by waiting for the expansion of the ion-wake channel to take the ion-wake radius to the chosen value.

For outlining the detailed physics in the sections below, representative particle-in-cell (PIC) simulation snapshots in Figs. 1 and 2 illustrate the excitation phase and the propagation phase of the ion soliton, respectively. The detailed initial conditions and setup of the simulations are in Secs. III B and IV B. Figure 1 shows the excitation phase at an early time when the bubble wake train is still executing orderly oscillations and its fields have begun to excite inertial ion motion resulting in a solitonlike ion-wake structure ($\delta n_i/n_0 \simeq 0.2$) as seen in Figs. 1(b) and 1(c). At later times shown in Fig. 2 the radial

oscillations that sustain the bubble train have phase mixed, converting much of the plasma wave energy into electron thermal energy. The resulting electron thermal pressure drives the ion soliton ($\delta n_i/n_0 > 1$) outwards. The time evolution of the radial dynamics of the ion density structure driven by the bubble electron mode is shown in a movie in Supplemental Material [20].

It is important to note that this work builds upon several earlier works on related topics such as (i) on long time scale phase mixing of electron wakefield oscillations—estimation of phase-mixing time scales [21], heating of electrons in wakefields in finite radius plasma [22] and (ii) on ion motion in response to plasma electron wakefields—on-axis ion density spike excitation by the ponderomotive force of the wake of a laser pulse [23], excitation of an on-axis ion filament by the electron beam accelerated in a laser wakefield accelerator [24], ion motion in electron wakefields driven by self-modulated proton bunches [25]. The existence of a regime similar to the crunch-in regime of positron beams discussed here, using proton beams where fields just behind the driver are utilized, has been illustrated in [26]. The proton beam driven regime however does not show a nonlinear surface wave unlike shown in the work of the author [9,10]. The nonlinear surface wave allows using accelerating and focusing fields much further behind the driver.

The paper is organized into the following sections. Section II uses the linearized fluid equations for modeling the ion dynamics to show the two distinct phases of the ion wake: the excitation phase and the propagation phase. We use an analytical model based on the fields of a nonlinear bubble plasma wave and simulations to demonstrate the inertial phase of the ion wake in Sec. III, while the fields of the bubble persist. Once the fields die out to nearly a hundredth of their initial value and the wake electrons thermalize into a non-isothermal spatial distribution sustaining radial electron temperature gradients supported by the electrostatic forces of electron-ion charge separation, we show that the driven nonlinear ion-acoustic waves is in the form of a cylindrical ion soliton. In Sec. IV the propagation phase of the ion wake is analytical modeled with simulations verifying the propagation of the cylindrical ion soliton driven by the radial temperature gradient of the phase-mixed electrons. Finally, in Sec. V we introduce and analyze the properties of the crunch-in regime driven by a relativistic positron beam in an ion-wake channel, using an analytical model and simulations. In the Appendix we present considerations and assumptions made to derive the ion-wake model.

II. ION WAKE: A DRIVEN PLASMA ION WAVE

To develop insight into the ion wake physics, we consider the 1D simplified dispersion relation of the ion-acoustic plane waves,

$$\omega^2 = \frac{c_s^2 k^2}{1 + (c_s/\omega_{\rm pi})^2 k^2}, \tag{1}$$

where $\omega_{\rm pi} = \omega_{\rm pe}\sqrt{m_e/m_i}$ and $c_s = \sqrt{k_B T^e_{\rm wk}/m_l}$ under the collisionless condition, $T^i_{\rm wk} \ll T^e_{\rm wk}$ and $\Upsilon = 1 + 2/f$ is the adiabatic index with f being the degrees of freedom of the ions.

At early times the ion motion is dominated by inertia, thus ions move over the plasma-ion time scales when driven by time varying and asymmetric phases of the fields of nonlinear electron plasma-wave (asymmetry of the phases is shown in Figs. 3 and 4). Thus initially, $\omega \simeq \omega_{\rm pi}$ and the ion density spike grows over the plasma-ion frequency time scales, $2\pi\omega_{\rm pi}^{-1}$. The radial electron oscillations sustaining the bubble undergo phase mixing [21], the electron trajectories lose orderly motion and thermalize. As the electrons thermalize, the ion motion is driven by thermal pressure of electrons.

The tendency of the thermal pressure of the electrons to expand outwards leads to charge separation electric field due to ion inertia and thus imparts a significant momentum to the ions. However, the interplay between electron thermal pressure and the ion electrostatic force gets the ions oscillating over larger spatial scales. In this thermally driven phase, the acoustic wave propagation becomes dispersionless with $\omega = kc_s$.

An ion-acoustic wave growing in amplitude undergoes self-steepening, forming a density spike over much smaller spatial scales; k becomes large while dispersion becomes important. The ion wake modeled here is nonlinear, thus the large k dispersion relation retaining the higher-order terms in k in the Taylor series expansion of Eq. (1) is $\omega = c_s k - 0.5 c_s \lambda_{De}^2 k^3$.

At much later times, the ions undergo heating; as T_i increases, the sound speed modifies to $c_s = \sqrt{k_B(\Upsilon_e T_e + \Upsilon_i T_i)/m_i}$.

A. Time-scale separation of ion dynamics: Soliton excitation and propagation

We illustrate the time-scale separation of the nonlinear electron mode using a PIC simulation snapshot over tens of electron oscillations behind the driver in Fig. 3. In Fig. 3(a) the coherent motion in the first four or five oscillations behind the driver is evident; whereas further behind the driver, the electrons begin to decohere due to phase mixing [21].

To understand how these electron oscillations couple to the ion mode we derive the ion-wave equation for the ion wake in the linear fluid approximation driven by two terms: the coherent electron mode and the electron thermal pressure. The linearized ion acoustic wave can be obtained by perturbative expansion of ion density, n_i and ion fluid velocity v_i in the ion fluid continuity equation,

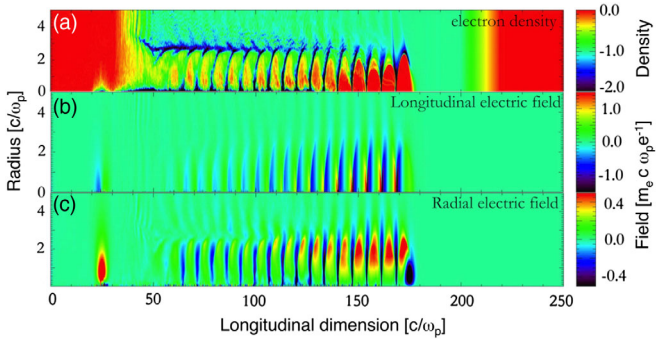

FIG. 3. Bubble-wake train behind an ultrarelativistic electron beam with bubble: $\beta_g \ll \beta_\phi \simeq \beta_{\rm beam}$. (a) Electron density in 2D cylindrical real space, (b) corresponding longitudinal electric field profile and (c) corresponding radial-field profile. Here the beam is located between 170 and 180 $\frac{c}{\omega_{\rm pe}}$. The bubbles just behind the driver in (a) undergo phase mixing over several cycles. The intermediate stages of the extent of phase mixing can be inferred from the bubbles that are closer to the beam. The beam-plasma parameters are the same as in Fig. 2 but the electron wake is shown at an earlier time $t = 150\omega_{\rm pe}^{-1}$.

$n_0 \boldsymbol{\nabla}\cdot\mathbf{v}_i^{(1)} + \frac{\partial n_i^{(1)}}{\partial t} = 0$. Taking a partial derivative with time, $\boldsymbol{\nabla}\cdot\frac{\partial \mathbf{v}_i^{(1)}}{\partial t} + \frac{\partial^2}{\partial t^2}\frac{n_i^{(1)}}{n_0} = 0$. The ion-fluid equation of motion where the electron temperature (T_e) has a spatial gradient and electron mode electric field ($\mathbf{E}_{\rm wk}$) still persist is $m_i \frac{\partial \mathbf{v}_i^{(1)}}{\partial t} = eZ_i\mathbf{E}_{\rm wk} - \Upsilon k_B T_e \boldsymbol{\nabla}\frac{n_i^{(1)}}{n_0} - \Upsilon k_B \frac{n_i^{(1)}}{n_0}\boldsymbol{\nabla}T_e$. The assumption of spatial gradient of electron temperature has been used because electron plasma wave oscillations phase mix into nonisothermal plasma (this is substantiated through numerical results in the simulations section in Fig. 5). Upon substituting the equation of motion in the time derivative of the linearized continuity equation, $\boldsymbol{\nabla}\cdot\left(\frac{eZ_i}{m_i}\mathbf{E}_{\rm wk} - \frac{\Upsilon k_B T_e}{m_i}\boldsymbol{\nabla}\frac{n_i^{(1)}}{n_0} - \frac{\Upsilon k_B}{m_i}\frac{n_i^{(1)}}{n_0}\boldsymbol{\nabla}T_e\right) + \frac{\partial^2}{\partial t^2}\frac{n_i^{(1)}}{n_0} = 0$. Thus, a driven ion-acoustic wave linearized to the first order in density perturbation has the form

$$\left(\frac{\partial^2}{\partial t^2} - c_s^2\nabla^2\right)\frac{n_i^{(1)}(\mathbf{r},t)}{n_0} = -\frac{eZ_i}{m_i}\boldsymbol{\nabla}\cdot\mathbf{E}_{\rm wk}(\mathbf{r},t)\Big|_{\rm wake} + \frac{\Upsilon k_B}{m_i}\frac{n_i^{(1)}}{n_0}\nabla^2 T_e\Big|_{\rm thermal}.$$

In this first-order approximate ion-fluid model the right-hand side of Eq. (2) shows two separate time scales of the ion wake.

At earlier times, the first term on the right-hand side dominates. This is the *formation or inertial* phase of the ion wake where the bubble electron oscillations undergo ordered radial motion and the bubble radial electric field excites the inertial response of the ions. The group velocity of the electron bubble wake ($\beta_g \approx 3v_{\rm th}^2/c^2$, in the 1D limit, where $v_{\rm th} \simeq \sqrt{k_B T_e/m_e}$ is the mean electron thermal velocity [27–29]) is much smaller than the phase velocity so the bubble fields interact with the background plasma over several oscillations. Figure 3 shows the nonlinear electron-wake train [electron density in real space in 3(a)] and its time-asymmetric fields [longitudinal 3(b) and radial 3(c)] driven by a near speed-of-light energy source of high intensity. The fields lead to the formation of the on-axis and R_B ion density spikes. At later times after the phase mixing between radial oscillators the electrons thermalize and $\mathbf{E}_{\rm wk}(\mathbf{r},t) \sim 0$. This is the *propagation or thermal* phase where the electron thermal pressure gradient drives the cylindrical soliton around R_B radially outwards to many times R_B.

Equation (2) is used to demonstrate the separation of ion response over two different time scales (its solution only describe the linear ion modes). In the inertial or excitation phase when the plasma is cold ($T_e \simeq 0$, $c_s \simeq 0$), a better description is provided by an ion-ring model driven by the fields of the electron wave. The ion-ring model is developed and verified using PIC simulations in Sec. III. The thermally driven propagation phase is modeled as a driven ion-acoustic soliton and verified by PIC simulations in Sec. IV.

The falling off of the electron mode fields to nearly zero as the electrons thermalize is later shown using PIC simulations over a much longer time scale in Sec. IV [see Fig. 6(b) where the radial electric field goes to zero around $200\omega_{\rm pe}^{-1}$ and the ion soliton is seen moving outwards radially in 6(a)].

There is another way to appreciate the separation of ion-wake dynamics into two phases: (i) in the inertial phase ion rings move in response to the fields of the wake, sustained primarily by electron motion. We model the ion dynamics using a kinetic theory approach and an ion-ring model has been presented to study the motion of ions resulting from different ion rings taking individual trajectories in response to the spatially varying forces. (ii) In the thermal phase where the collective fields nearly vanish, we expect a fluid theory approach to dominate the modeling of the dynamics, but there is still some kinetic behavior which affects the ion motion. However, during the thermal phase the dominant behavior is more fluidlike with higher-order corrections from the residual kinetic effects.

III. EXCITATION PHASE: ION INERTIAL RESPONSE TO THE BUBBLE FIELDS

Since the characteristic time of ion motion is much longer than the electron oscillations, the longitudinal field $\mathbf{E}_{\rm wk}\cdot\hat{z}$ averages out over one full bubble electron oscillation in time. In other words the net change in the spatial average of the potential over the bubble is zero (from the Panofsky-Wenzel theorem). So, the ions gain relatively small net longitudinal momentum. However, atypical radial

ion dynamics arise because the radial fields, $\mathbf{E}_{\rm wk}\cdot\hat{r}$ are asymmetric in time as shown in Fig. 4 and drive radial ion momentum which does not average to zero, resulting in an average radial ion momentum. It is shown here that the ions are driven into a solitonlike density buildup which stably propagates radially over many hundreds of electron periods (shown in Sec. IV).

A. Ion-ring analytical model: Interaction with time-asymmetric bubble radial fields

The first stage of the ion-wake formation is controlled by the different time-asymmetric phases of ion dynamics inertially responding to the bubble radial field impulses shown in Fig. 4, namely, "suck-in" due to the electron compression in the back of the bubble $F^{\rm back}$ during $\tau_{\rm back}$ shown in Fig. 4(c), and the "push-out" due to the mutual-ion space-charge Coulomb repulsion force $F^{\rm sc}$ during τ_{cav} shown in Fig. 4(d). The crunch-in force is spatially periodic at nonlinear plasma wavelength, $\lambda_{\rm Np}\approx 2R_B$ with a duty cycle $\mathcal{D}=\frac{\tau_{\rm back}}{\tau_{\rm back}+\tau_{\rm cav}}\ll 1$. It is important to note that even though the duration of the radial forces in the two phases are highly asymmetric, their magnitudes are nearly equal [seen by comparing Figs. 4(c) and 4(d)].

In addition to the forces from the electron wake, the propagating energy sources themselves impart impulses such as the laser ponderomotive force $F^{pm}\tau_{\rm las}$ ($\tau_{\rm las}$ is laser pulse duration), where $F_e^{pm}(r,z)=-\frac{m_e c^2}{2\gamma_e}\nabla_{r,z}|\mathbf{a}(r)|^2$ (γ_e is the plasma electron Lorentz factor) and the radial force of the drive beam $F_b\tau_b$, where $F_b(r)=-2\pi e^2 n_b r$. The short

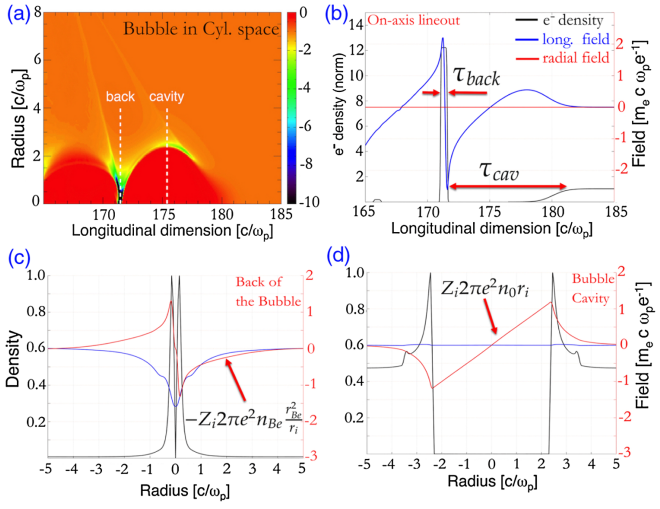

FIG. 4. Ion dynamics in longitudinally asymmetric phases of the radial forces in an electron bubble. (a) Electron density of a bubble in 2D cylindrical real space. (b) Longitudinal on-axis profile of the electron density (black), longitudinal field (blue), focusing field (red). (c) Radial-field profile close to the back of the bubble. This is the focusing suck-in phase for the ions. (d) The fields at the center of the ion cavity of the bubble. This is the defocusing "push-out" phase for the ions.

driver impulses are neglected (beam density here is below threshold intensity for direct nonlinear ion excitation [7]) because they act on the ions over their subwavelength short duration. This is unlike the slowly propagating wake-plasmon bubbles that undergo continual interaction over many plasma periods. The validity of this assumption is evident from the laser ion wake in Fig. 1. Since the ponderomotive force of a laser driver is an outward force for both the electrons and ions, the on-axis density spike cannot be from this direct force from the laser. Similarly the ion-density spike at the radial wake edge in an electron beam driven ion motion cannot be excited directly by the space-charge force of the beam, and is caused by the electron wake's radial-edge density compression.

The Lagrangian model of the ions in a bubble consists of ion rings under cylindrical symmetry with $m_i d^2 r_i/dt^2=\Sigma F_{\rm wk}$ (where $F_{\rm wk}$ is the force of the electron wake on the ions). The bared-ion region inside the bubble is assumed to be a positively charged cylinder under steady-state approximation ($R_B > r_{\rm Be}$, back of the bubble electron compression radius). The force on the ions from the nonlinear electron compression $\delta n_e = n_{\rm Be}\gg n_0$ in the back of the bubble and radius $r_{\rm Be}$ pulls the ion rings towards the axis; and within the bubble, the mutual space-charge force of the ion rings leads to them being driven outwards, away from the axis. The suck-in force on the ions is $F^{\rm back}=-Z_i 2\pi e^2 n_{\rm Be}\frac{r_{\rm Be}^2}{r_i}$. The space-charge force on the ions in the cavity is $F^{\rm sc}=Z_i 2\pi e^2 n_0 r_i$. The equation of motion is $m_i d^2 r_i/dt^2-\frac{c\beta_\phi}{\lambda_{\rm Np}}(F^{\rm sc}\tau_{\rm cav}-F^{\rm back}\tau_{\rm back})=0$ using $\omega_{\rm pi}^2=Z_i 4\pi e^2 n_0/m_i$, we have

$$\frac{d^2 r_i}{dt^2}+\beta_\phi\frac{\omega_{\rm pi}^2}{2}\left(\frac{n_{\rm Be}}{n_0}\frac{\tau_{\rm back}}{\tau_{\rm cav}}\frac{r_{\rm Be}^2}{r_i^2}-1\right)r_i=0, \qquad (2)$$

where we have assumed that $c\tau_{\rm cav}/\lambda_{\rm Np}\simeq 1$. Therefore the ion dynamics is dictated by an equilibrium or a separatrix ion-ring radius, where the inward and the outward impulses balance out, $r_i^{\rm eq}=r_{\rm Be}\sqrt{\frac{n_{\rm Be}}{n_0}\mathcal{D}}$. The ion rings at $r_i\le r_i^{\rm eq}$ collapse inwards towards the axis resulting in an on-axis density spike, whereas the ion rings at $r_i\ge r_i^{\rm eq}$ move out away from the axis. For $m_i/Z_i > m_p$ the ion response is slower but similar.

When the radially outward moving ion rings reach beyond R_B, there is excess net negative charge of the wake electrons within the bubble sheath. As a result the radially outwards propagating ion rings pushed initially by the bubble forces cannot freely escape the bubble sheath and slow down to start accumulating just inside the bubble sheath, forming a density compression at R_B. So, the cylindrical ion soliton is formed around R_B. This accumulation of the moving ion rings is shown in Fig. 1, where it is seen that the ion and electron density start forming a peak at R_B.

The radial location of the excitation of the ion soliton in the nonlinear electron-wave regime is much greater than a skin depth, $c/\omega_{\rm pe}$; thus the ion wake starts off with a spatial scale which is over several $c/\omega_{\rm pe}$. This is due to the balance of opposing radial forces on the plasma electrons from the driver and the ion cavity, resulting in their radial accumulation at R_B [4]. In the laser-driven case, the outward ponderomotive force is balanced by the evacuated ion cavity: $F^{pm}_{\rm las} = -\frac{m_e c^2}{2\gamma_e}\nabla_r|\mathbf{a}_0(r)|^2 \simeq F_{\rm cav} = 2\pi e^2 n_0 R_B$ gives $R_B \sim (c/\omega_{\rm pe})^2 \frac{1}{\gamma_e}\nabla_r|\mathbf{a}_0(r)|^2$ when simplified using $\nabla_r|\mathbf{a}_0(r)|^2 \simeq a_0^2/R_B$ and $\gamma_e \simeq a_0$, $R_B \simeq \sqrt{a_0}\frac{c}{\omega_{\rm pe}}$ (computationally, $\simeq 2\sqrt{a_0}c/\omega_{\rm pe}$ [4,30]). In the electron beam-driven bubble the outward force of the beam on the plasma electrons is balanced by the inward pull of the evacuated ion cavity: $F_b(R_B) = 2\pi e^2 n_b r_b^2/R_B \simeq F_{\rm cav} = 2\pi e^2 n_0 R_B$. This gives, $R_B \simeq \sqrt{\Lambda_b/(\pi n_0)}$ [30], where $\Lambda_b = n_b \pi r_b^2$ is the line charge density of the beam, where r_b is the beam radius computed here as $2.3\sigma_r$ to account for 95% of beam particles for a radially Gaussian beam profile.

B. Bubble field time-asymmetry driven ion soliton: Simulation results

The above ion-ring model is verified using $2\frac{1}{2}D$ OSIRIS PIC simulations [31] of the ion wake in the bubble regime by simulating various energy sources–laser pulses in Cartesian coordinates and electron beams in cylindrical coordinates. The laser pulse is circularly polarized with Gaussian radial and longitudinal profile with $a_0 = 4$ (not shown $a_0 = 1.0$ to 40.0), pulse length of $30\frac{1}{\omega_0}$, matched focal spot-size radius of $40\frac{c}{\omega_0}$, and laser frequency $\omega_0 = 10\omega_{\rm pe}$ (the pulse dimensions are in the FWHM of the field). The electron beam is initialized with $\gamma_b \sim 38,000$, $n_b = 5n_0$ (not shown $n_b = 0.25n_0$ to $50n_0$) and spatial Gaussian distribution with $\sigma_r = 0.5\frac{c}{\omega_{\rm pe}}$ and $\sigma_z = 1.5\frac{c}{\omega_{\rm pe}}$ (the beam spatial dimensions are 5σ in both dimensions). The smallest spatial scale, $c/\omega_{\rm pe}$ is resolved in the beam case and c/ω_0 in the laser case (laser frequency ω_0), with 20 cells in the longitudinal direction and 50 cells in the transverse direction. Each of the plasma grid cells has 36 particles. The beam is initialized with 64 particles per cell. The plasma is initialized in the Eulerian specification (non-moving window) and preionized with $Z_i = 1$. At the longitudinal boundaries we initialize vacuum space of $50c/\omega_{\rm pe}$ followed by density ramps of $20\ c/\omega_{\rm pe}$ sandwiching the homogeneous plasma [32]. Absorbing boundary conditions are used for fields and particles.

The electron-beam driven ion-wake soliton structure in theory is compared to the simulations in Figs. 4(a) and 3(a). We observe $R_B = 2.45c/\omega_{\rm pe}$ (just behind the beam), whereas the estimated bubble radius is $R_B = \sqrt{n_b/n_0(2.3\sigma_r)^2} = 2.57c/\omega_{\rm pe}$ ($r_b = 2.3\sigma_r = 1.15c/\omega_{\rm pe}$, the assumption $r_b \ll R_B$ is not strictly satisfied). In Fig. 2 which is in the propagation phase, the observed ion-wake soliton is located at $r \simeq 3.3c/\omega_{\rm pe}$ at $460\omega_{\rm pe}^{-1}$ which is about $1.7\frac{2\pi}{\omega_{\rm pi}}$. The ion soliton is excited at an early time around R_B and in the snapshot in Fig. 2 it has propagated outwards. The on-axis density spike drops to a minimum at $r_i^{\rm eq} \approx 0.45c/\omega_{\rm pe}$ in Fig. 2 whereas the estimated $r_i^{\rm eq} = 0.5c/\omega_{\rm pe}$ ($n_{\rm Be}/n_0 \simeq 12$, $\mathcal{D} \simeq 0.1$, $r_{\rm Be} \simeq 0.5c/\omega_{\rm pe}$). The radial ion momentum $p_r - r$ phase space in Fig. 7(b) shows the ions accumulate at the axis and the channel edge, at a time corresponding to Fig. 2(b). The ions at the channel edge are seen to have a drift velocity and a thermal spread. The radial electron momentum $p_r - r$ phase space in Fig. 7(a) shows that a large density of thermalized electrons are trapped within the ion soliton which is confirmed from the density plots in Fig. 2(a).

In the laser-driven bubble simulations the expected and observed $R_B \simeq 4c/\omega_{\rm pe}$ as shown in Fig. 1(a). In Fig. 1(c) the ion-wake soliton is created at $r = 4.2c/\omega_{\rm pe}$. The expected and observed on-axis density-spike radius is $r_i^{\rm eq} = 0.45c/\omega_{\rm pe}$ ($n_{\rm Be}/n_0 \simeq 8$, $\mathcal{D} \simeq 0.1$, $r_{\rm Be} \simeq 0.5c/\omega_{\rm pe}$). The model for the excitation of this structure of the nonlinear wake has been verified for a range of laser and beam parameters from quasilinear to strongly nonlinear electron wake regime.

IV. PROPAGATION PHASE: SOLITON DRIVEN BY ELECTRON THERMAL PRESSURE GRADIENT

As described in Sec. III the electron bubble–wake train fields excite a cylindrical ion soliton. Eventually, the electron oscillations phase mix and thermalize as electron thermal energy on the time scale of about an ion plasma period. In light of this ongoing thermalization process over the evolution of the ion wake, we note that the terminology of temperature is not exact until phase mixing is complete and individual electrons have lost any synchronization in time and space. However, as the energy in the decohering wake electrons has the tendency of radial outflow, for simplicity it may be characterized as thermal energy.

In this section we model the propagation of the cylindrical soliton radially outwards driven by the temperature (or wake electron energy) gradient as modeled in Eq. (3). This soliton propagation is modeled using a modified cKdV equation in a nonequilibrium condition such that an electron temperature gradient sustains and drives the cylindrical ion soliton.

A. Analytical model: Thermally driven ion-acoustic soliton

In the linear regime the homogenous ion-acoustic wave equation predicts sinusoidal radial ion oscillations that support the wave. However, the linearized ion-acoustic wave equation is inadequate to describe the propagating

solitary ion density spike at the edge of the ion-wake, with ion density accumulation many times the background density.

When the density in the ion perturbation begins to rise to the order of the background density, the electrostatic potential due to charge separation between the ions and the thermal electrons correspondingly rises. This leads to *wave steepening* due to the preferential acceleration of ions in the direction of the ion-acoustic wave velocity. When the potential of the wave is large enough the ions get trapped and copropagate at the ion-acoustic wave phase velocity, this nonlinearity is the basis of the soliton. It should be noted that the linearized kinetic theory does not formally incorporate the trapping of particles at the wave phase velocity. In this limit the density perturbation shape is therefore not sinusoidal as the copropagating background ions accumulate and their density perturbation takes the form of an ion soliton. The copropagating ion velocity in the soliton can therefore exceed the ion-acoustic phase velocity, $v_i > c_s$ and $\mathcal{M} - 1 > 0$ where $\mathcal{M} = v_i/c_s$ is the Mach number. Therefore, nonlinear acoustic waves are in the form of a soliton and propagate faster than the ion-acoustic velocity.

To the second order, the nonlinear ion-density spike $n_i(r,t) > n_0$ propagation is governed by the Korteweg–de Vries (KdV) equation [14] which has propagating solutions of the form $\mathcal{U}(r - \mathcal{M}c_s t)$ [13] where $\mathcal{U}$ is the ion-acoustic waveform, a soliton solution and $\mathcal{M}$ is the Mach number $(= v_i/c_s)$ of the propagating solution. Higher-order contributions to the KdV equation have also been considered by earlier works. However, the more important and relevant consideration here is that the standard form of the cKdV equation assumes an isothermal plasma whereas the bubble

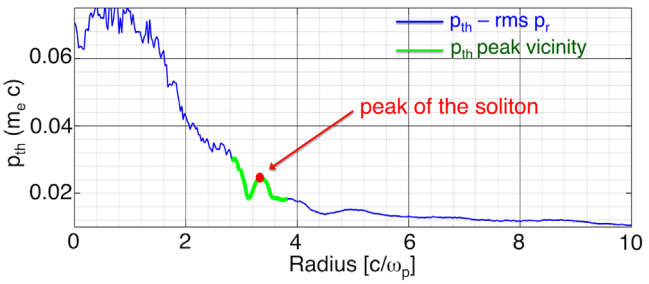

FIG. 5. Radial profile of the root-mean-square radial electron momentum (proportional to the square root of the electron temperature, $\sqrt{T_e}$) at 460 $\omega_{\rm pe}^{-1}$ for the beam-driven ion wake in Fig. 2. The blue curve shows the root-mean-squared radial electron momentum, $p_{\rm th}^e(r) = \sqrt{[\Sigma_k p_r^2(k,r) 2\pi r n_e(k,r)]/\Sigma_k 2\pi r n_e(k,r)}$ profile of the wake electrons corresponding to the time in Fig. 2 at 460 $\omega_{\rm pe}^{-1}$. This represents the square root of the electron temperature, $p_{\rm th}^e \propto \sqrt{T_e}$. The radial gradient of the temperature, $\frac{\partial}{\partial r} T_e$ is thus computed at the peak of the soliton (red) and in its vicinity (green). It is interesting to note that $\frac{\partial}{\partial r} T_e^{(1)}|_{\rm peak} = 0$.

wake phase mixes into a plasma with a radial electron temperature gradient, whereas the ions are initially cold. In a nonisothermal plasma the effect of trapped electrons in the ion soliton have been considered using the Bernstein-Greene-Kruskal model at the ion-acoustic velocity [33].

It is also known that a single ion soliton under the appropriate conditions can break up into multiple solitons leading to a N-soliton solution [29]. N-solitons are a train of multiple solitons that are supported by the soliton equations because the entire train is a solution too. This is also a phenomenon we observe in the simulations shown in the ion density of the beam-driven case at $z = 60\frac{c}{\omega_{\rm pe}}$ in Fig. 2.

We consider a description of the nonlinear cylindrical ion-acoustic waves with a radial temperature gradient. We assume that the background electron trapping does not significantly modify the distribution function. We assume that the temperature changes slowly in the vicinity of the ion soliton. This assumption is validated by the PIC simulations in Fig. 5.

To obtain the KdV equation [18] in cylindrical coordinates (cKdV) with radial temperature gradient we normalize with respect to the local electron temperature, the radius: $\hat{r} = \frac{r}{\lambda_D}$; time: $\hat{t} = \omega_{\rm pi} t = t\sqrt{\frac{4\pi e^2 n_0}{m_i}}$; electric field: $\hat{E} = \frac{e\lambda_{De}}{k_B T_e} E$; potential: $\phi = \frac{e}{k_B T_e}\Phi$; ion-density perturbation: $\hat{n}_i = n_i/n_0$; electron-density perturbation: $\hat{n}_e = n_e/n_0$; ion-fluid velocity: $\hat{v} = \frac{v_i}{c_s}$. Under this normalization the cylindrical coordinate equations transform as electron Boltzmann distribution equation $\frac{\partial \hat{n}_e}{\partial \hat{r}} = -\hat{n}_e \hat{E} - \hat{n}_e \phi \frac{\partial}{\partial \hat{r}} \ln T_e$, ion-fluid continuity equation $\frac{\partial}{\partial \hat{t}} \hat{n}_i + 2\frac{\hat{n}_i \hat{v}}{\hat{r}} + 2\frac{\partial}{\partial \hat{r}} \hat{n}_i \hat{v} = 0$, ion-fluid equation of motion $\frac{\partial}{\partial \hat{t}} \hat{v} + \hat{v}\frac{\partial}{\partial \hat{r}} \hat{v} = \hat{E}$ and the Poisson equation $\nabla^2 \Phi = \frac{1}{\hat{r}} \frac{\partial}{\partial \hat{r}} (\hat{r}\hat{E}) = \hat{n}_i - \hat{n}_e$. The electric field $\hat{E}$ is both due to the thermal pressure and the radial fields of the wake, $\hat{E}_{\rm wk} + \hat{E}_{\rm th}$. But, in the following analysis the propagation of a nonlinear ion-acoustic wave is considered, so we assume that the electron oscillations are thermalized and thus the effect of the fields of the wake is negligible, $\hat{E}_{\rm wk} \to 0$ (to the second order).

We look for a propagating disturbance of $\hat{n}_e$, $\hat{n}_i$, $\hat{v}$ and $\hat{E}$ in a stationary background plasma with uniform background density n_0. We consider weakly nonlinear ion-acoustic wave and expand all the wave quantities in the powers of $\delta = \mathcal{M} - 1$. We perturbatively expand $\hat{n}_i$, $\hat{n}_e$, $\hat{E}$, ϕ, T_e and $\hat{v}_i$ and retain all terms up to the order of δ^2. Note that we have assumed that before the electron wake excitation the plasma is cold, $T_e^{(0)} \simeq 0$.

We transform to a moving frame of the steepened ion density perturbation using the coordinate transform $\xi = \delta^{1/2}(\hat{r} - \hat{t})$ and $\tau = \delta^{3/2}\hat{t}$. Using this, $\hat{r} = \delta^{-1/2}(\xi + \delta^{-1}\tau)$ and $\frac{\partial \xi}{\partial \tau} = \frac{\partial \xi}{\partial \hat{t}}\frac{\partial \hat{t}}{\partial \tau} = -\frac{1}{\delta}$. We renormalize the electric field as $\tilde{E} = \delta^{-1/2}\hat{E}$. Note that in the moving frame the potential

gradient is $E = -\frac{\partial}{\partial \hat{r}}\Phi = -\delta^{1/2}\frac{\partial}{\partial \xi}\Phi$, so $\tilde{E}$ is a more appropriate quantity.

Under the assumption that in the moving frame the quantities of the disturbance change with small $\delta = \mathcal{M} - 1$, the terms in equations are perturbatively expanded and the terms with same powers of δ are collected. From the δ^1 order terms of all the equations above, it is inferred that $\Phi^{(1)} = n_e^{(1)} = v^{(1)} = n_i^{(1)} \equiv \mathcal{U}$ and $\frac{\partial}{\partial \xi}\mathcal{U} = -\tilde{E}^{(1)}$.

By collecting the δ^2 terms from the Boltzmann's equation we obtain $\tilde{E}^{(2)} = -\frac{\partial}{\partial \xi}n_e^{(2)} + \mathcal{U}\frac{\partial}{\partial \xi}\mathcal{U} - \mathcal{U}\frac{\partial}{\partial \xi}T_e^{(1)}$. Similarly, collecting the δ^2 terms from the ion-fluid equation of motion we obtain $\frac{\partial}{\partial \xi}\hat{v}^{(2)} - \frac{\partial}{\partial \xi}n_e^{(2)} = \frac{\partial}{\partial \tau}\mathcal{U} + \mathcal{U}\frac{\partial}{\partial \xi}T_e^{(1)}$ and from the Poisson equation we obtain $\frac{\partial^3}{\partial \xi^3}\mathcal{U} = -\frac{\partial}{\partial \xi}(n_i^{(2)} - n_e^{(2)})$. Taking the δ-order terms of the continuity equation and substituting $\mathcal{U}$ we obtain $\mathcal{U} + \tau\left(\frac{\partial}{\partial \tau}\mathcal{U} + 2\mathcal{U}\frac{\partial}{\partial \xi}\mathcal{U} + \left[\frac{\partial}{\partial \xi}v^{(2)} - \frac{\partial}{\partial \xi}n_e^{(2)}\right]\right) - \delta(U^2 + v^{(2)}) = 0$. Neglecting quantities with δ times the second-order terms and using the $\frac{\partial}{\partial \tau}\mathcal{U}$ result above, $\frac{\mathcal{U}}{\tau} + 2\frac{\partial}{\partial \tau}\mathcal{U} + 2\mathcal{U}\frac{\partial}{\partial \xi}\mathcal{U} + [\frac{\partial}{\partial \xi}n_e^{(2)} - \frac{\partial}{\partial \xi}n_i^{(2)}] = -\mathcal{U}\frac{\partial}{\partial \xi}T_e^{(1)}$.

Using the δ^2 terms of the Poisson equation in the above result and using the self-similarity property of the ion soliton, we obtain the driven Korteweg–de Vries equation in cylindrical coordinates [11] (a more detailed derivation of this modified cKdV model can be found in [18]),

$$\Phi^{(1)} = n_e^{(1)} = v^{(1)} = n_i^{(1)} \equiv \mathcal{U}$$
$$\frac{\mathcal{U}}{\tau} + 2\frac{\partial}{\partial \tau}\mathcal{U} + 2\mathcal{U}\frac{\partial}{\partial \xi}\mathcal{U} + \frac{\partial^3}{\partial \xi^3}\mathcal{U} = -\mathcal{U}\frac{\partial}{\partial \xi}T_e^{(1)}. \quad (3)$$

It differs from the Cartesian-KdV equation by the term $\frac{\mathcal{U}}{\tau}$ and the temperature-gradient based driver term $-\mathcal{U}\frac{\partial}{\partial \xi}T_e^{(1)}$. The Cartesian KdV equation can be analytically solved to obtain two classes of solutions: (a) self-similar solutions which are shown in [13] to be Airy functions and (b) soliton solutions. A "soliton" is a single isolated pulse which retains its shape as it propagates at some velocity, v_{soliton}. This means that for a solitonlike solution $\mathcal{U}$ only depends upon the soliton-frame variable, $\zeta = \xi - \mathcal{M}c_s\tau$ and not on spacelike ξ and timelike τ variables separately. The solution of the Cartesian KdV equation in this comoving frame is $\mathcal{U}(\zeta) = 3v_s\text{sech}^2(\sqrt{\frac{v_s}{2}}\zeta)$ [13].

The cKdV equation and the driven cKdV equation obtained here cannot be solved analytically. However, earlier numerical analysis and experimental verification [12] of the cylindrical-KdV (cKdV) equation show that it supports functions of the form $\mathcal{U} \propto \text{sech}^2(r - \mathcal{M}c_s t)$ in the form of a cylindrical ion soliton. But, the amplitude of the cylindrical soliton changes as it propagates. The velocity of the soliton in the cylindrical case is higher than in the Cartesian case [11]. Since the ion wake is excited in a nonisothermal plasma its velocity changes as it is driven. The mean electron temperature reduces as the soliton propagates radially outwards because the electron thermal energy is distributed over a larger volume, thus as the drive weakens the soliton slows down.

We have numerically solved the driven-cKdV equation, Eq. (3) and as expected, when the right-hand side is set to zero, the amplitude of an outwards propagating ion soliton asymptotically decreases over time. However, when the driving term is present the soliton amplitude stabilizes or undergoes growth depending upon the initial temperature. Note that the integrated thermal energy is held constant in these numerical analyses. Thus, this work shows that the wake electron temperature gradient radially drives the ion soliton for much longer distances than possible in an isothermal plasma.

The cKdV equation is also known to support an N-soliton solution, and simulations show N-soliton forming during the propagation phase. We computationally seek the dependence of the nonlinear ion-density spike on the $(r - \mathcal{M}c_s t)$-coordinate.

It should be noted that such soliton solutions are supported under certain limiting conditions on the Mach number, $\mathcal{M}$. The strict condition on the existence and stability of ion soliton arises from a threshold limit on the magnitude of soliton potential to continue trapping the background ions.

Here we find that the speed of the ion soliton is nearly equal to and only slightly higher that the ion-acoustic speed calculated using the mean temperature. As this is not an isothermal plasma, there is no well-defined ion-acoustic speed. So, the ion-acoustic wave is phase mixed and its velocity also changes as it propagates.

The local electron temperature of the ion soliton, as shown in Fig. 5, is used to calculate the Mach number $\mathcal{M}$ and thus a stability criterion can be derived. This problem is represented using the condition on the Sagdeev pseudopotential, $\mathcal{V}(\phi) = -[\exp(\phi) - 1 + \mathcal{M}(\mathcal{M}^2 - 2\phi)^{1/2} - \mathcal{M}^2]$ that it has to be a real number. This condition is satisfied when $\mathcal{M}^2 - 2\phi \geq 0$; therefore, $\phi < \mathcal{M}^2/2$ and $\phi_{\max} = \mathcal{M}^2/2$. Using this we find the well-known condition,

$$1 < \mathcal{M} < 1.6, \qquad v_i < 1.6c_s$$
$$\phi < \frac{\mathcal{M}_{\max}^2}{2} = 1.28. \quad (4)$$

As will be shown later, we find from simulations that the Mach number calculated using the mean temperature is well within these bounds, and thus the soliton is stable.

B. Simulation results: Thermally driven ion-acoustic soliton

The channel-edge density spike, with a form similar to the cKdV solution in the $r - \mathcal{M}c_s t$ frame as shown in

Figs. 1 and 2 is seen to be propagating radially outwards. The propagation phase starts around $t = 200\omega_{pe}^{-1}$ as the radial electric fields $\mathbf{E}_{wk} \to 0$ as shown in Fig. 6(b). The propagation phase is evident in Fig. 6(a) where the red curve is the position of the peak of the ion soliton in time. The radial position of the peak of the ion soliton from each of the PIC electrons and ion density snapshot is obtained in the postprocessing scripts and this is shown in Fig. 6(a). The cylindrical ion soliton has propagated from $r_{soliton}(460\omega_{pe}^{-1}) = 3.3c/\omega_{pe}$ (also seen in Fig. 2) to $r_{soliton}(1100\omega_{pe}^{-1}) = 4.1c/\omega_{pe}$ which corresponds to an average speed of $\langle v_{soliton}\rangle = 0.0013c$.

We compare the time-averaged soliton speed $\langle v_{soliton}\rangle$ to the average speed of sound, $c_s/c = p_{th}^{e}\sqrt{\frac{\Upsilon}{2}\frac{m_e}{m_i}}$, where the average $p_{th}^{e} \simeq 0.06$ from the electron phase space (not shown). This gives $c_s \simeq 0.001c$ ($\Upsilon = 2$ for 2D) in agreement with the average soliton velocity. Using this time-averaged analysis we see that $\mathcal{M} \simeq 1.3$ and so the stability criteria in Eq. (4) is satisfied.

However, as the soliton moves out the volume between the axis and the soliton edge increases. Thus the electron thermal energy redistributes and spreads over a larger volume. This leads to the reduction in the temperature with time. The soliton is not freely propagating but is driven by the radial gradient of the electron temperature as shown in Eq. (3). The soliton speed thus changes in time as shown in the red curve of Fig. 6(c). The sound speed also varies with time and it is estimated using the temperature at that instant using $c_s(t) = \sqrt{k_B\langle T_e(t)\rangle/m_i}$. The plasma is not in thermal equilibrium and its temperature varies radially as shown in Fig. 5. The root-mean-square radial momentum is used to estimate the temperature at any instant of time, and is

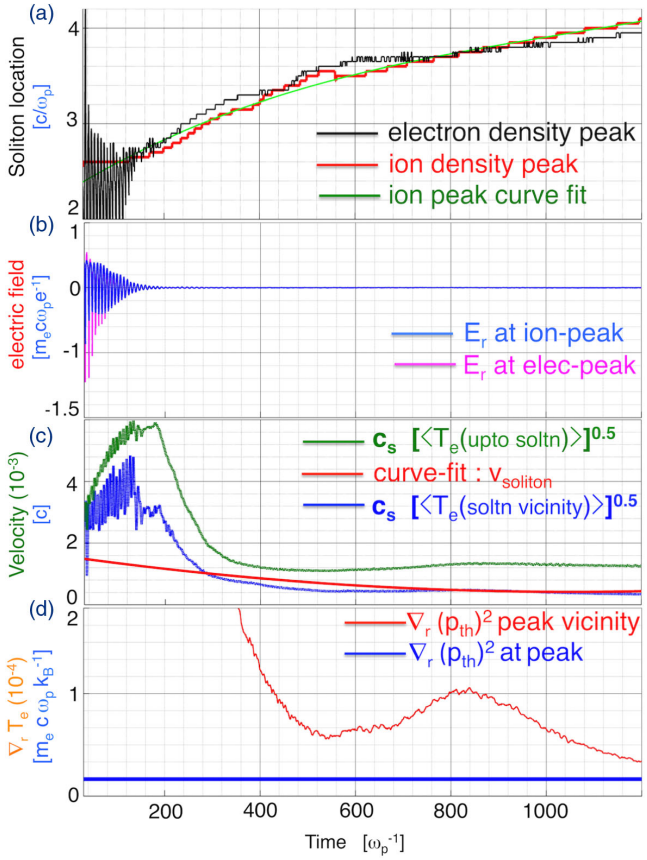

FIG. 6. Time evolution of the cylindrical ion soliton. (a) Electron (black) and ion (red) spike radial positions (in terms of $c\omega_{pe}^{-1}$) with time and a third-order fit (green) for the position of the ion density-spike of the soliton. (b) Radial fields of the electron bubble oscillations (in terms of $m_e c\omega_{pe}e^{-1}$) at the electron density spike (magenta) and at the ion density spike (blue). (c) Radial velocity of the ion density spike of the soliton calculated from the third-order fit curve (red). An estimate of the sound speed (green) using the mean temperature, between the axis and the soliton location (green) and in the vicinity of the soliton peak (blue), in the expression $c_s = \sqrt{k_B\langle T_e\rangle/m_i}$. Since the plasma is not isothermal the mean temperature is calculated by averaging the temperature of electrons over the indicated spatial region. (d) Gradient of the electron temperature at the soliton ion density peak (blue) and in the vicinity of the peak (red). The vicinity of the ion density peak of the soliton is defined as shown in Fig. 5.

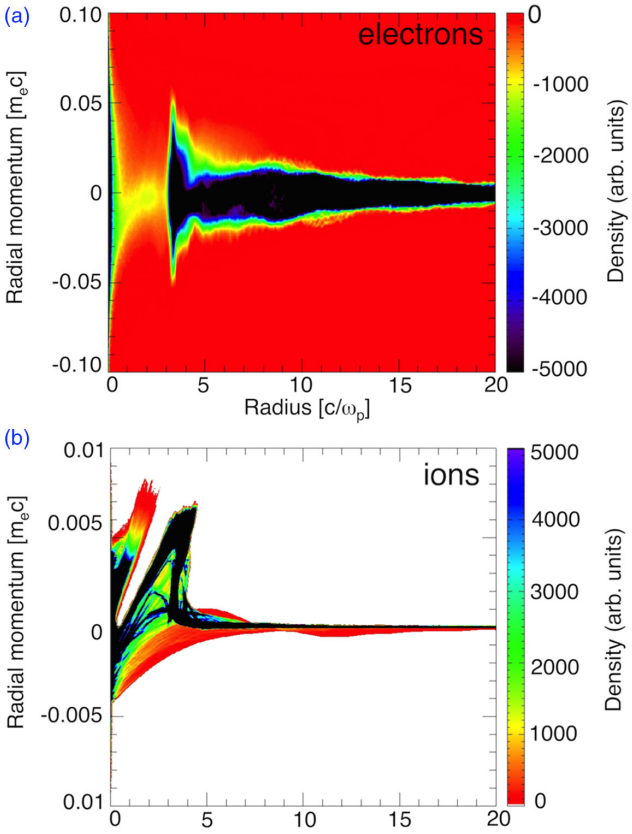

FIG. 7. Radial phase-space snapshots of the electron and ion density in Fig. 2. (a) Electron $p_r - r$ radial momentum phase space showing the accumulation of thermalized electrons within the ion soliton. (b) Ion $p_r - r$ radial momentum phase space showing the on-axis and ion-wake edge ion accumulations.

calculated over radial dimension from the $p_r - r$ phase space. The mean temperature is calculated by taking the average of the rms radial momentum—over the entire channel: channel-$\langle p^e_{\rm th}\rangle = [\Sigma^{r_{\rm sol}}_{r=0} p_{\rm th}(r) 2\pi r n_e(r)]/\Sigma^{r_{\rm sol}}_{r=0} 2\pi r n_e(r) \propto$ channel $-\sqrt{\langle T_e\rangle}$ or in the vicinity of the soliton: soliton-$\langle p^e_{\rm th}\rangle = [\Sigma^{r_{\rm sol}+\epsilon}_{r_{\rm sol}-\epsilon} p_{\rm th}(r) 2\pi r n_e(r)]/\Sigma^{r_{\rm sol}+\epsilon}_{r_{\rm sol}-\epsilon} 2\pi r n_e(r) \propto$ soliton $-\sqrt{\langle T_e\rangle}$. The instantaneous sound speed, $c_s(t)$ computed with channel-$\langle p^e_{\rm th}\rangle$ is in the green curve in Fig. 6(c) and $c_s(t)$ computed with soliton-$\langle p^e_{\rm th}\rangle$ is in the blue curve in Fig. 6(c). The extent of the vicinity (ϵ) around the soliton peak is shown in Fig. 5.

We compare the curves in (i) red: $v_{\rm soliton}(t)$ (from the third order polynomial curve fit of the radial position of the ion-density peak as a function of time); (ii) green: $c_s(t)$ from channel-$\langle p^e_{\rm th}(t)\rangle$; and (iii) blue: $c_s(t)$ from soliton-$\langle p^e_{\rm th}(t)\rangle$ in Fig. 6(c). From the comparison it is observed that they are in good agreement. It can be seen that the velocity of the soliton estimated using the location of the ion-density peak (red) lies between $c_s(t)$ calculated using the average temperature over the channel (green) which is the upper limit and $c_s(t)$ calculated using the average temperature over the soliton (blue) which is the lower limit.

We also present the radial gradient of the electron temperature, $\frac{\partial}{\partial r} T_e(r,t)$ in Fig. 6(d). It is interesting to note from the blue curve in Fig. 6(d) that the temperature gradient at the peak of the ion soliton is zero, $\frac{\partial}{\partial r} T_e(r,t)\Big|_{\rm peak} = 0$. In the vicinity of the soliton peak we see that the gradient of the temperature follows the variation in the ion soliton velocity, this follows from Eq. (3). The vicinity of the soliton peak is shown as the green curve overlaid on the thermal momentum curve in Fig. 5.

In Fig. 2(b) N-soliton formation is observed in the ion density at around $z \simeq 60\frac{c}{\omega_{\rm pe}}$. The single-ion soliton is seen splitting into several solitons. The N-soliton solution can be explained by the seeding of different initial momentum of the ion rings because ion rings driven in the push-out phase have a radial position dependent defocusing force acting on them, $F^{\rm sc}(r_i) = Z_i 2\pi e^2 n_0 r_i$. This is shown in Fig. 4(d). Thus the ion rings originating at a larger radii from the axis are pushed outwards with a force of a higher magnitude and the rings originating at a smaller radii just outside $r^{\rm eq}_i$ are pushed outwards by a smaller force. So, over a longer time the set of ion rings with a higher initial momentum propagate radially outwards at a larger radial velocity. This break-up of a single ion soliton into N-solitons occurs over a longer time scale because the difference in momentum is small compared to the average momentum.

The thermal momentum, $p^{\rm th}_e$, at this time is less than one-tenth of the peak wake quiver momentum. There are several reasons for the cooling, such as transfer of the wake energy to the ions and the trapped electrons [32], escape of the highest energy electrons and untrapped ions from the channel edge, the thermal heat flux, energy loss to the bow-shock and the redistribution of the energy over an expanding volume. The peak radial ion momentum is $\simeq$0.005 which shows that not all the radially propagating ions are trapped. The untrapped free-streaming ions at $\simeq 7c/\omega_{\rm pe}$ can be distinguished from the ions at the channel edge in $p_r - r$ phase space.

It should be noted that the long-term stability of the on-axis ion-density spike of the nonlinear ion-acoustic wave is not fully modeled here. The on-axis ion-density spike will disintegrate due to mutual Coulomb repulsion of the ions over the sub-skin-depth spike radius. This effect of the collapse of the on-axis density spike will be addressed in future work. We expect that the disintegration of the central structure to be further by azimuthal asymmetries not included in the cylindrically symmetric simulations. Earlier disintegration is seen in Cartesian simulations shown in [18].

In summary, the ion wake is a near-void channel with sub-skin-depth density spikes on axis and at the bubble edge located at the bubble radius, R_B of several $c/\omega_{\rm pe}$. The ion accumulation in both the density spikes is many times the background density, and the outer spike propagates outwards as a solitary structure at slightly above the speed of sound.

The time scale of dissipation of ion wake and relaxation of the plasma distribution to $v_{\rm th}/c \sim 0$ sets an upper limit on the repetition rate [17] of the future plasma colliders. In our PIC based analysis, the ion soliton is tracked up to time duration of around 3000 $\omega^{-1}_{\rm pe}$, which is used to infer an upper limit on repetition rate of the order of 0.5 ns. It is well known that the ion acoustic wave is damped by collisions and ion-wave Landau damping. The ion dynamics opens questions upon the plasma container walls and the distance needed from the beam axis to avoid damaging them by the significant radially outward ion flux. We leave a more complete answer for the dissipation of the ion wake and equilibration of the plasma for future work.

It was earlier suggested that the electron-mode energy in the plasma wave could be replenished and sustained [34] by a train of energy source in order to achieve high repetition rate. However, as shown in this paper due to ion motion this is not possible.

V. CRUNCH-IN REGIME IN THE ION-WAKE CHANNEL

We explore the use of the ion-wake channel for positron-beam driven plasma acceleration of particle beams in a novel and relevant crunch-in regime [9,10]. This regime requires that the hollow-channel (n_0 density outside channel and 0 density inside it, with a Heaviside function like transition) radius be matched to the beam properties, which requires meter-scale channel of a few $c/\omega_{\rm pe}$ radius, this condition is indeed satisfied by the ion-wake channel.

Hollow channels are promising [35,36] for exciting the well-studied purely electromagnetic electron modes based

on particle currents on the surface of walls. These pure electromagnetic fields driven in a hollow channel have proven to have zero focusing forces when driven by relativistic particles [36]. In the crunch-in regime the on-axis focusing forces originate from the on-axis compression of electrons which produce a field that pull positrons towards the axis.

Here we show that in the crunch-in regime driven even in an ion-wake channel, strong accelerating and focusing fields of electrostatic nature are excited by the electron rings crunching in from the channel wall. The ion wake enables the crunch-in regime because as it slowly propagates radially outwards, the channel radii scans over a broad range of coefficients of c/ω_{pe}, while its length is the energy-source plasma interaction length. Meter-scale propagation of electron beams and few centimeter-scale propagation of laser beams in plasmas while exciting nonlinear bubble electron waves have been well characterized in experiments. The theoretical model presented above thus provides a mechanism to generate long channels of several skin-depth radii. As we show below, the excitation of nonlinear crunch-in regime requires such channels to optimally match with the driving energy source.

It is well known [37] that in a homogeneous plasma positron beam driven wakes have two major problems [9]: (i) The plasma electrons collapsing to the axis from different radii arrive at different times, preventing optimal compression. This is because the radial force of the positron beam driving the crunch-in decreases with the radii. (ii) The plasma ions located in the path of the positron beam result in a defocusing force on it. The transport of positrons in a positron-beam driven wake is thus not ideal in a homogenous plasma. The use of ion-wake channels with a few c/ω_{pe} is shown here to provide possible pathways to overcome these fundamental problems.

The formation of much shorter plasma channels excited by significantly different processes have been shown previously. These processes include using a collimated laser with annular profile [38], using a hollow capillary discharge [39], among others [23,40].

A. Analytical model: Nonlinearly driven ion-wake channel

Positron acceleration using the ion-wake channel which is a realization of a hollow channel is explored in the nonlinear crunch-in regime of perturbed electron oscillation radii, $\delta r_e \geq r_{ch}$, under the condition that the peak beam density $n_{pb} > n_0$. Here we intend to show that the radial electron motion which sustains the nonlinear cylindrical surface mode has the characteristics that the on-axis electron collapse time depends on beam properties in addition to the channel radius.

An analytical model of the radial electron suck-in based excitation of a positron beam wake in a homogeneous plasma is developed in [37]. The equation of motion of the plasma electron rings at r from the axis, under the electrostatic force of a positron beam, neglecting the space-charge force of the collapsing electron rings is $\frac{d^2}{d\xi^2} r \propto -\frac{1}{r} n_{bp}(\xi) r_{bp}^2(\xi)$, where $\xi = c\beta_{pb} t - z$ is the space just behind the positron beam with velocity $c\beta_{pb}$ driving the collapse. This is under an assumption about the positron-beam properties, $n_{bp}(\xi)$ and $r_{bp}(\xi)$ being constant during the entire interaction of the positron beam with the hollow channel over its full length. The solution to this equation is [9] $r_{ch}\sqrt{\pi}\mathrm{erf}[\sqrt{\ln(r_{ch}/r)}] = -\sqrt{2\mathcal{C}}\xi$, where $\mathcal{C} = \frac{1}{2\pi\beta_b^2}\frac{n_{bp}}{n_0}\pi(\frac{r_{bp}}{c/\omega_{pe}})^2$. Therefore, the collapse time duration is $\xi_{coll} = -r_{ch}\sqrt{\frac{\pi}{2\mathcal{C}}}$. The collapse time in a homogeneous plasma is [37]

$$\tau_c = \sqrt{\pi}\frac{r_{ch}}{\omega_{pe}\sqrt{n_{bp}/n_0}\, r_{pb}}. \tag{5}$$

We have used this expression to show that the collapse time even in a homogeneous plasma depends strongly on the properties of the beam and the radius from which the rings are collapsing in. This solution is however not applicable to the nonlinear hollow-channel regime, because the ion density only exists for $r > r_{ch}$. Also, note that we have neglected the initial expansion velocity of the channel, dr_{ch}/dt).

In a hollow channel for optimal compression of electrons avoiding phase mixing, the electron rings should collapse over $\tau_c \simeq \mathcal{D}\lambda_{Np}/c$, where λ_{Np} is the nonlinear wavelength of the positron-driven wake and $\mathcal{D}$ is the duty cycle of compression phase. So, the optimal channel radius is $r_{ch}^{opt} \simeq 2\sqrt{\pi}\mathcal{D}\frac{\lambda_{Np}}{\lambda_{pe}}\frac{\omega_{pb}}{\omega_{pe}} r_{pb}$. The scaling of the r_{ch}^{opt} with positron beam parameters is shown in [9].

B. Simulation result: Nonlinearly driven ion-wake channel

Using $2\frac{1}{2}D$ PIC simulations in a moving window we study the positron beam driven fields in cylindrical hollow-channel plasma. We compare positron acceleration in an ideal [Heaviside density function, $n_0\mathsf{H}(r - r_{ch})$] and an ion-wake channel (with on-axis and channel-edge density spike, channel minimum density of $0.1n_0$) with $r_{ch} = 2.5c/\omega_{pe}$, under fixed-ion assumption. For nonlinear wake parameters $r_{pb} = 2.3c/\omega_{pe}$, $n_{pb} = 1.3n_0$ and $r_{ch}^{opt} \simeq 2.3c/\omega_{pe}$ ($\mathcal{D}\frac{\lambda_{Np}}{\lambda_{pe}} = 0.25$).

The radial variation of the fields presented in Fig. 8(b) at the peak longitudinal field shows that the peak on-axis accelerating field is $0.4m_e c\omega_{pe}e^{-1}$ for an ideal channel and $0.2m_e c\omega_{pe}e^{-1}$ for the ion-wake channel with an on-axis density spike. Figure 8 also shows that the potential of the focussing force (normalized to 27.6 $m_e c^2 e^{-1}$) is similar and overall focusing in both cases. However, in the ion channel

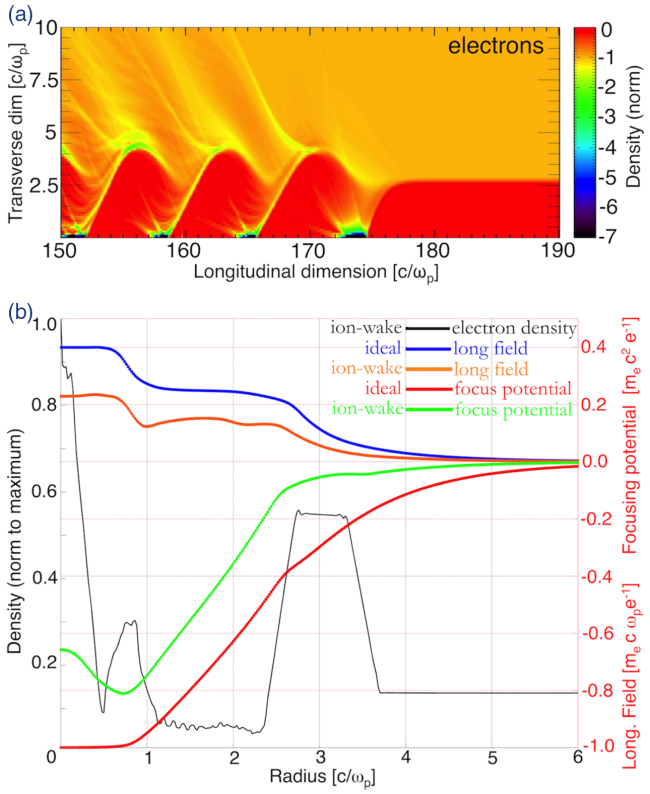

FIG. 8. 2D-PIC simulations: (a) electron density in real space showing electron density excitation in the crunch-in regime; (b) corresponding radial profile of fields excited by a positron beam in an ideal-channel versus an ion-wake channel. The radial profile of the normalized electron density (black) in an ion-wake channel (normalized to the maximum electron compression) at longitudinal location of the peak accelerating field ($r_{\mathrm{pb}} = 2.3c/\omega_{\mathrm{pe}}$, $\gamma_{\mathrm{pb}} = 380\,00$, $n_{\mathrm{pb}} = 1.3n_0$). The radial profile of the accelerating field and the normalized potential of the focusing field (E_r-B_θ) (radial field integrated from the edge of the box to a radius on x-axis).

the radial field is defocusing around the on-axis ion spike (on-axis spike collapses at later times).

We note that the on-axis density spike has a detrimental effect on the focusing fields near the axis. However, the on-axis density spike is unstable over longer time scales and collapses as shown in [18]. The cylindrical simulations used in the current work to model the ion wake ignore any azimuthal asymmetries in the distribution of electrons and ions in the on-axis density spike. Exploring the collapse of the on-axis density spike will be addressed in future work. Ideal channels of a few c/ω_{pe} are technologically challenging whereas the ion-wake channel of radius $r_{\mathrm{ch}} \gtrsim R_B$ is formed behind every bubble electron wake.

VI. CONCLUSION

In conclusion, using theory and PIC simulations we have shown the dynamics of the formation and evolution of a nonlinear ion wake excited by the time-asymmetric nature of electron bubble fields independent of the type of energy source. We have shown that the nonlinear ion wake has the characteristics of a cylindrical ion-soliton solution continuously driven by temperature gradient and evolves to an N-soliton solution over longer time as described by a driven cKdV equation. Thus over the period of persistence of the ion soliton, a second electron bunch cannot be accelerated in the plasma. We have tracked the ion soliton over a time scale of thousands of plasma electron periods which corresponds to hundreds of picosecond for 10^{17} cm^{-3} plasma electron densities. This establishes an upper limit on the repetition rate of a plasma collider of at least many hundreds of picoseconds for plasma electron densities around 10^{17} cm^{-3}. We have also shown the feasibility of using the ion-wake channel for positron acceleration in the positron-beam driven crunch-in regime within an experimentally relevant parameter regime.

ACKNOWLEDGMENTS

This work was supported by the U.S. Department of Energy under Grant No. DE-SC0010012 and the National Science Foundation under Grant No. NSF-PHY-0936278. I am immensely grateful to Professor T. Katsouleas for providing several comments on the physics and writing style of this manuscript and the same applies to all the referees. I acknowledge the geniality of the research group of Prof. Z. Najmudin within the Department of Physics at the Imperial College London and the John Adams Institute for Accelerator Sciences, where I have been based while making corrections to the manuscript during its review. I acknowledge the OSIRIS collaboration [31] for providing the PIC code for the simulations presented here. I acknowledge support for experiments by FACET group within the E-224 collaboration at Stanford Linear Accelerator Laboratory and Professor M. Downer's group at University of Texas at Austin, with special thanks to Dr. R. Zgadzaj. I also acknowledge the 256-node *Chanakya* server at Duke university.

APPENDIX: CONSIDERATIONS IN THE NONLINEAR ION-WAKE MODEL

There are several considerations and assumptions that underlie the nonlinear ion-wake model. Here we briefly describe these and seek to differentiate the ion wake from other phenomena. Primarily, we establish that the ion wake is a collisionless phenomena and it is significantly different from diffusion. Second, as the ion wake is formed behind the high phase-velocity nonlinear electron plasma waves that are excited by the fields of near speed of light propagating energy sources, it is significantly different from hole-boring which occurs while the energy source has near-zero group velocity.

We recognize that to study the time evolution of a wake-excited plasma, for establishing the duration over which it

relaxes to thermal equilibrium, both collisional and collisionless dynamics have to be considered along with the physics of recombination modes such as electron-ion recombination. However, in this work the dynamics of plasma is modeled under the collisionless approximation. Thus, diffusion is not important during the time scales over which the ion wake is studied. We do not discuss recombination except mentioning that the "afterglow" is dominated by volume recombination while localized effects appearing in this work cannot be ruled out.

In order to formally establish the difference between the density wave processes that occur over collisionless time scale in contrast to the ones that start dominating under collisions, we show the assumptions made to arrive at the dynamics of diffusion. The process of diffusion is modeled with a parabolic partial differential equation which is deduced from the ion-fluid equations under the assumption that the inertial response of the ions is much faster than the collisional time scales.

The effect of collisions is introduced as a drag force, $m_i n \nu_{\rm coll} \langle \vec{v}_i \rangle$. The collisional drag force modifies the ion-fluid equation of motion as $m_i n_i \frac{d\vec{v}_i}{dt} = m_i n_i (\frac{\partial \langle \vec{v}_i \rangle}{\partial t} + \langle \vec{v}_i \rangle \vec{\nabla} \cdot \langle \vec{v}_i \rangle) = \pm e n \vec{E} - \vec{\nabla} \mathcal{P}_e - m_i n_i \nu_{\rm coll} \langle \vec{v}_i \rangle$ where $\nu_{\rm coll}$ is the average electron-ion collision frequency and is obtained from the mean-free path. Diffusion of plasma is thus driven by the charge-separation field, $\vec{E}$, and the thermal pressure, $\mathcal{P}_e$, while being impeded by the collisional drag. Upon ignoring the inertia of the ions, $\frac{\partial \vec{v}_i}{\partial t} = 0$, the equation for the ion velocity by diffusion in an isothermal plasma is $\langle \vec{v}_i \rangle = \pm \frac{e}{m \nu_{\rm coll}} \vec{E} - \frac{k_B T_e}{m \nu_{\rm coll}} \frac{\vec{\nabla} n_i}{n_0}$. The characteristic parameter of diffusion is the diffusion coefficient or diffusivity $D = \frac{k_B T_e}{m \nu_{\rm coll}}$ and mobility $\mu = \frac{e}{m \nu_{\rm coll}}$ which depend upon the collision frequency. Using the gradient of the velocity in the continuity equation and ignoring the mobility, μ, leads to a Fick's law diffusion equation, $\nabla^2 \frac{n_i}{n_0} \propto \frac{\partial}{\partial t} \frac{n_i}{n_0}$, characteristic of a parabolic equation.

When the mobility is retained, the fluid equation is a moment of the Fokker-Planck equation which is the kinetic model of the collision-driven drift and diffusion. The diffusion equation thus cannot support a wavelike solution because such solutions are characteristic of a hyperbolic partial differential equation.

The solutions of linear and nonlinear diffusion equations show the evolution of density profile by diffusion and can be obtained using the self-similar formulation. The self-similar solutions show the spatial and temporal evolution of the density to be exponentially decaying. In the nonlinear case, the density can have a sharp front as it decays. However, a solitonlike propagating solution cannot be described with the diffusion equation. Hence, the cylindrical ion soliton presented here is not diffusion but a wave phenomenon.

The electron bubble wake is excited by a subwavelength impulse of an ultrashort driver. In contrast, the ion wake is excited as the ions undergo sustained interactions with the bubble fields within the spatial extent of the wake over several plasma electron oscillations. This happens because the electron wake-plasmon oscillations [28] have a near speed-of-light phase velocity ($\beta_\phi \simeq 1$) but negligible group velocity [27] $\beta_g \approx 3 v_{\rm th}^2/c^2$ (in the 1D limit), where $v_{\rm th} \simeq \sqrt{k_B T_e/m_e}$ is the mean electron thermal velocity of the background plasma. Therefore a slowly propagating train of coupled electron plasmons is excited in a cold collisionless plasma [27]. A large difference between phase velocity and the group velocity of the electron oscillations allows sustained field-ion interactions. It should be noted that high phase-velocity plasma electron waves are possible only in a cold plasma with appropriate density, n_0, that allows near speed-of-light propagation of the energy sources, $\beta_{es} \simeq 1 \approxeq \beta_\phi$. The ion soliton modeled here is assuming a significant difference between the phase velocity and the group velocity of the plasma-electron waves.

A time symmetric electron mode would excite time symmetric ion oscillations where the ion velocities average to zero. However, the bubble wake is asymmetric in time as the back of the bubble electron compression is a small fraction of the length of electron cavitation. The electron oscillations become nonlinear at high driver intensities as all the interacting electrons are displaced radially, $\delta n_e/n_0 > 1$, forming a nonlinear bubble-shaped electron spatial structure enclosing ions in its cavity. The fields excited in the bubble are useful for accelerating electrons [5,15,16]. High intensities also lead to fields that can directly drive the plasma electrons to velocities near the speed of light. This occurs when for a laser pulse $a_0 \geq 1$ and an electron beam $\frac{n_b}{n_0} (\frac{r_b}{c/\omega_{\rm pe}})^2 \geq 1$, where a_0 is the peak normalized laser vector potential, n_b, r_b the peak beam density and radius. The radially expelled electrons oscillate radially under the force of the plasma ions. These oscillations are excited over plasma electron oscillation time scales, $2\pi\omega_{\rm pe}^{-1}$ ($\omega_{\rm pe} = \sqrt{4\pi n_0 e^2/\gamma_e m_e}$), where $\gamma_e \beta_e m_e c$ is the temporally anharmonic relativistic electron quiver momentum. The normalized quiver momentum of the electrons in the bubble oscillations is relativistic $\gamma_\perp \beta_\perp \geq 1$ and the quiver frequency is $\omega_\perp = \omega_{\rm pe} (\frac{\beta_\phi^2}{\gamma(1-\beta_\phi^2)})^{1/2}$ [1].

We show that nonlinear ultrarelativistic electron-mode fields interacting with the plasma ions lead to the excitation of a nonlinear ion wake. The nonlinear ion wake $\delta n_i/n_0 > 1$ in Figs. 1 and 2 is excited over time scales $\gg 2\pi\omega_{\rm pe}^{-1}$ in the trail of a bubble-wake train. By shaping the energy source it can be matched or guided to excite a long train of nearly identical plasmons, Fig. 3. Since it is the electric field $\mathbf{E}_{\rm wk}$ of a nearly stationary bubble plasmon that excites collective ion motion we model the ion dynamics in a single bubble. Using the single bubble ion dynamics, Fig. 4, we model the ion wake over the whole bubble train spanning several hundred plasma skin depths ($c/\omega_{\rm pe}$).

The wake-plasmon energy density $\{\mathcal{E}_{\rm wk} = 0.5[e|\mathbf{E}_p|/(m_e c\omega_{\rm pe})]^2 m_e c^2 n_0$, where $\mathbf{E}_p$ is the plasma field amplitude$\}$ is continually partitioned between the field energy and the coherent electron quiver kinetic energy. In our model we do not include heavy beam loading of the bubble electron wake. Under heavy beam loading the bubble field energy is efficiently coupled to the kinetic energy of the accelerated beam. In this scenario the bubble collapses and the magnitude of the ion wake is smaller. The decoherence of the ordered electron quiver to random thermal energy, $\mathcal{E}_{\rm wk} \rightarrow k_B T_{\rm wk}$, due to the phase mixing [21] of individual electron trajectories caused by the nonlinearities and inhomogeneities is further stimulated by the ion motion. The details of the thermalization of the wake electrons under ion motion is beyond the scope of this paper. It is over these time scales upon thermalization that the steepened ion density expands outwards radially as a nonlinear ion-acoustic wave driven by the electron thermal pressure. The energy transfer process observed here is a coupling from the nonlinear plasma electron mode to a nonlinear ion-acoustic mode [8]. We also observe energy coupling to the bow-shock which is formed behind the bubble, Fig. 4, due to the trapped particles propagating faster than wave phase velocity.

[1] A. I. Akhiezer and R. V. Polovin, Theory of wave motion of an electron plasma, Zh. Eksp. Teor. Fiz., **30**, 915 (1956) [Sov. Phys. JETP **3**, 696 (1956)].

[2] T. Tajima and J. M. Dawson, Laser Electron Accelerator, Phys. Rev. Lett. **43**, 267 (1979); P. Chen, J. M. Dawson, R. W. Huff, and T. Katsouleas, Acceleration of Electrons by the Interaction of a Bunched Electron Beam with a Plasma, Phys. Rev. Lett. **54**, 693 (1985).

[3] G. Z. Sun, E. Ott, Y. C. Lee, and P. Guzdar, Self-focusing of short intense pulses in plasmas, Phys. Fluids **30**, 526 (1987).

[4] A. Pukhov and J. Meyer-Ter-Vehn, Laser wakefield acceleration: The highly nonlinear broken-wave regime, Appl. Phys. B **74**, 355 (2002).

[5] J. B. Rosenzweig, B. Breizman, T. Katsouleas, and J. J. Su, Acceleration and focusing of electrons in two-dimensional nonlinear plasma wakefields, Phys. Rev. A **44**, (1991).

[6] A. Seryi, M. Hogan, S. Pei, T. Raubenheimer, P. Tenenbaum, T. Katsouleas, C. K. Huang, C. Joshi, W. B. Mori, and P. Muggli, A concept of plasma wakefield acceleration linear collider (PWFA-LC), in *Proceedings of the 23rd Particle Accelerator Conference, Vancouver, Canada, 2009* (IEEE, Piscataway, NJ, 2009), WE6PFP081.

[7] J. B. Rosenzweig, A. M. Cook, A. Scott, M. C. Thompson, and R. B. Yoder, Effects of Ion Motion in Intense Beam-Driven Plasma Wakefield Accelerators, Phys. Rev. Lett. **95**, 195002 (2005).

[8] A. A. Sahai, T. C. Katsouleas, F. S. Tsung, and W. B. Mori, Long term evolution of plasma wakefields, in *Proceedings of the 25th Particle Accelerator Conference, PAC-2013, Pasadena, CA, 2013* (IEEE, New York, 2013), MOPAC10, ISBN: 978-3-95450-138-0.

[9] A. A. Sahai and T. C. Katsouleas, Optimal positron-beam excited wakefields in hollow and ion-wake channels, in *Proceedings of the International Particle Accelerator Conference, Richmond, Virginia, 2015*.

[10] A. A. Sahai, Crunch-in regime—Nonlinearly driven hollow-channel plasma, at the Advanced Accelerator Conference, 2016, MD, arXiv:1610.03289.

[11] Stephen Maxon and James Viecelli, Cylindrical solitons, Phys. Fluids **17**, 1614 (1974); Spherical Solitons, Phys. Rev. Lett. **32**, 4 (1974).

[12] Noah Hershkowitz and Thomas Romesser, Observations of Ion-Acoustic Cylindrical Solitons, Phys. Rev. Lett. **32**, 581 (1974).

[13] Yu. A. Berezin and V. I. Karpman, Theory of nonstationary finite-amplitude waves in a low-density plasma, Sov. Phys. JETP **19**, 1265 (1964) [Zh. Eksp. Teor. Fiz. **46**, 1880 (1964)].

[14] D. J. Korteweg and G. de Vries, On the change of form of long waves advancing in a rectangular canal, and on a new type of long stationary waves, Philos. Mag. **39**, 422 (1895).

[15] S. P. D. Mangles, C. D. Murphy, Z. Najmudin, A. G. R. Thomas, J. L. Collier, A. E. Dangor, E. J. Divall, P. S. Foster, J. G. Gallacher, C. J. Hooker *et al.*, Nature (London) **431**, 535 (2004); C. G. R. Geddes, Cs. Toth, J. van Tilborg, E. Esarey, C. B. Schroeder, D. Bruhwiler, C. Nieter, J. Cary, and W. P. Leemans, Nature (London) **431**, 538 (2004); J. Faure, Y. Glinec, A. Pukhov, S. Kiselev, S. Gordienko, E. Lefebvre, J.-P. Rousseau, F. Burgy, and V. Malka, Nature (London) **431**, 541 (2004).

[16] M. Litos, E. Adli, W. An, C. I. Clarke, C. E. Clayton, S. Corde, J. P. Delahaye, R. J. England, A. S. Fisher, J. Frederico *et al.*, High-efficiency acceleration of an electron beam in a plasma wakefield accelerator, Nature (London) **92**, 515 (2014).

[17] A. A. Sahai, T. C. Katsouleas, S. Gessner, M. Hogan, C. Joshi, and W. B. Mori, Excitation of wakefields in a relativistically hot plasma created by dying nonlinear plasma wakefields, AIP Conf. Proc. **1507**, 618 (2012).

[18] A. A. Sahai, On certain nonlinear and relativistic effects in plasma-based particle acceleration, Ph.D. dissertation, Duke University, 2015.

[19] T. C. Chiou and T. Katsouleas, High Beam Quality and Efficiency in Plasma-Based Accelerators, Phys. Rev. Lett. **81**, 3411 (1998).

[20] See Supplemental Material at http://link.aps.org/supplemental/10.1103/PhysRevAccelBeams.20.081004 for a movie of the radial dynamics of electron and ion density driven in the ion-wake channel of an electron-beam driven nonlinear electron wake (in MP4 format).

[21] S. SenGupta and P. K. Kaw, Phase Mixing of Nonlinear Plasma Oscillations in an Arbitrary Mass Ratio Cold Plasma, Phys. Rev. Lett. **82**, 1867 (1999).

[22] K. V. Lotov, A. P. Sosedkin, and A. V. Petrenko, Long-Term Evolution of Broken Wakefields in Finite-Radius Plasmas, Phys. Rev. Lett. **112**, 194801 (2014).

[23] L. M. Gorbunov, P. Mora, and A. A. Solodov, Plasma Ions Dynamics in the Wake of a Short Laser Pulse, Phys. Rev.

Lett. **86**, 3332 (2001); L. M. Gorbunov, P. Mora, and A. A. Solodov, Dynamics of a plasma channel created by the wakefield of a short laser pulse, Phys. Plasmas **10**, 1124 (2003).

[24] K. I. Popov, W. Rozmus, V. Yu. Bychenkov, N. Naseri, C. E. Capjack, and A. V. Brantov, Ion Response to Relativistic Electron Bunches in the Blowout Regime of Laser-Plasma Accelerators, Phys. Rev. Lett. **105**, 195002 (2010).

[25] J. Vieira, R. A. Fonseca, W. B. Mori, and L. O. Silva, Ion Motion in Self-Modulated Plasma Wakefield Accelerators, Phys. Rev. Lett. **109**, 145005 (2012).

[26] L. Yi, B. Shen, K. Lotov, L. Ji, X. Zhang, W. Wang, X. Zhao, Y. Yahong, J. Xu, X. Wang, Y. Shi, L. Zhang, T. Xu, and Z. Xu, Scheme for proton-driven plasma-wakefield acceleration of positively charged particles in a hollow plasma channel, Phys. Rev. ST Accel. Beams **16**, 071301 (2013); L. Yi, B. Shen, L. Ji, K. Lotov, A. Sosedkin, X. Zhang, W. Wang, J. Xu, Y. Shi, L. Zhang, and Z. Xu, Positron acceleration in a hollow plasma channel up to TeV regime, Sci. Rep. **4**, 4171 (2015).

[27] A. A. Vlasov, The vibrational properties of an electron gas, Zh. Eksp. Teor. Fiz. **8**, 291 (1938) [Sov. Phys. JETP **93**, 3 (1968)].

[28] L. Tonks and I. Langmuir, Oscillations in ionized gases, Phys. Rev. **33**, 195 (1929).

[29] F. F. Chen, *Introduction to Plasma Physics and Controlled Fusion* (Plenum Press, New York, 1983), ISBN-13:978-0306413322.

[30] W. Lu, M. Tzoufras, C. Joshi, F. S. Tsung, W. B. Mori, J. Vieira, R. A. Fonseca, and L. O. Silva, A nonlinear theory for multidimensional relativistic plasma wave wakefields, Phys. Plasmas **13**, 056709 (2006).

[31] R. A. Fonseca, L. O. Silva, F. S. Tsung, V. K. Decyk, W. Lu, C. Ren, W. B. Mori, S. Deng, S. Lee, T. Katsouleas, and J. C. Adam, OSIRIS, a three-dimensional fully relativistic particle in cell code for modeling plasma based accelerators, in *International Conference on Computational Science*, edited by P. M. A. Sloot *et al.*, Lecture Notes in Computer Science Vol. 2331, (Springer, Heidelberg, 2002), p. 342.

[32] A. A. Sahai, T. C. Katsouleas, and P. Muggli, Self-injection by trapping of plasma e^- oscillating in rising density gradient at the vacuum-plasma interface, *Proceedings of IPAC2014, Dresden, Germany*, TUPME51.

[33] H. Schamel, Stationary solitary, snoidal, and sinusoidal ion acoustic waves, Plasma Phys. **14**, 905 (1972).

[34] R. D. Ruth, A. D. Chao, P. L. Morton, and P. B. Wilson, A plasma wakefield accelerator, Part. Accel. **17**, 171 (1985).

[35] T. C. Chiou and T. C. Katsouleas, High Beam Quality and Efficiency in Plasma-Based Accelerators, Phys. Rev. Lett. **81**, 3411 (1998).

[36] C. B. Schroeder, D. H. Whittum, and J. S. Wurtele, Multimode Analysis of the Hollow Plasma Channel Wakefield Accelerator, Phys. Rev. Lett. **82**, 1177 (1999).

[37] S. Lee, T. C. Katsouleas, R. G. Hemker, E. S. Dodd, and W. B. Mori, Plasma-wakefield acceleration of a positron beam, Phys. Rev. E **64**, 045501 (2001).

[38] C. G. Durfee and H. M. Milchberg, Light Pipe for High Intensity Laser Pulses, Phys. Rev. Lett. **71**, 2409 (1993).

[39] R. F. Hubbard, Y. Ehrlich, D. Kaganovich, C. Cohen, C. I. Moore, P. Sprangle, A. Ting, and A. Zigler, Intense laser pulse propagation in capillary discharge plasma channels, AIP Conf. Proc. **472**, 394 (1999).

[40] A. Ting, C. I. Moore, K. Krushelnick, C. Manka, E. Esarey, P. Sprangle, R. Hubbard, H. R. Burris, R. Fischer, and M. Baine, Plasma wakefield generation and electron acceleration in a self-modulated laser wakefield accelerator experiment, Phys. Plasmas **4**, 1889 (1997); A. Ting, H. R. Burris, E. Esarey, J. Krall, P. Sprangle, K. Krushelnick, and C. I. Moore, Naval Research Laboratory Report No. NRL/MR/6790-96-7876, 1996.